Reflectance spectroscopy with polarized light: is it sensitive to cellular and nuclear morphology

Konstantin Sokolov, Rebekah Drezek, Kirk Gossage, and Rebecca Richards-Kortum

Biomedical Engineering Program, University of Texas, Austin, TX 78712

Abstract: We present a method for selective detection of size-dependent scattering characteristics of epithelial cells *in vivo* based on polarized illumination and polarization sensitive detection of scattered light. We illustrate the method using phantoms designed to simulate squamous epithelial tissue and progressing to epithelial tissue *in vitro* and *in vivo*. Elastic light scattering spectroscopy with polarized illumination/detection dramatically reduces background signals due to both diffuse stromal scattering and hemoglobin absorption. Resulting spectra can be described as a linear combination of forward and backscattering components determined from Mie theory. Nuclear sizes and refractive indices extracted by fitting experimental spectra to this model agree well with previous measurements. Reflectance spectroscopy with polarized light can provide quantitative morphological information which could potentially be used for non-invasive detection of neoplastic changes.

OCIS codes: (290.0290) Scattering; (170.6510) Spectroscopy, tissue diagnostics

References and links

1. American Cancer Society (1993) Cancer Facts and Figures. *Publication No. 93-400M, No. 5008-03*.
2. J. R. Mourant, T. Fuselier, J. Boyer, T.M. Johnson, and I.J. Bigio, "Predictions and Measurements of Scattering and Absorption Over Broad Wavelength Ranges in Tissue Phantoms," Appl. Opt. **36**, 949-57 (1997).
3. L.T. Perelman, V. Backman, M. Wallace, G. Zonios, R. Manoharan, A. Nusrat, S. Shields, M. Seiler, C. Lima, T. Hamano, I. Itzkan, J. Van Dam, J.M. Crawford, and M.S. Feld, "Observation of Periodic Fine Structure in Reflectance from Biological Tissue: A New Technique for Measuring Nuclear Size Distribution," Phys. Rev. Lett. 80, 627-630 (1998).
4. R.R. Anderson, "Polarized Light Examination and Photography of the Skin," Arch. Dermatol. **127**, 1000-5 (1991).
5. http://omlc.ogi.edu/news/feb98/polarization/index.html
6. V. Backman, R. Gurjar, K. Badizadegan, I. Itzkan, R. Dasari, L.T. Perelman, and M.S. Feld, "Polarized Light Scattering Spectroscopy for Quantitative Measurements of Epithelial Cellular Structures *In Situ*," IEEE, J. Selected Topics in Quantum Electronics on Lasers in Medicine and Biology **5**, (1999).
7. T.M. Johnson and J.R. Mourant, "Polarized Wavelength-Dependant Measurements of Turbid Media," Opt. Express 4, 200-216 (1999).
8. V. Sankaran, K. Schönenberger, J.T. Walsh, Jr., and D.J. Maitland, "Polarization Discrimination of Coherently Propagating Light in Turbid Media," Appl. Opt. **38**, 4252-4261 (1999).
9. G. Jarry, E. Steimer, V. Damaschini, M. Epifanie, M. Jurczak, and R. Kaiser, "Coherence and Polarization of Light Propagating Through scattering Media and Biological Tissues," Appl. Opt. **37**, 7357-7367 (1998).
10. D. Bicout, C. Brosseau, A.S. Martinez, J.M. Schmitt, "Depolarization of Multiply Scattered Waves by Spherical Diffusers: Influence of the Size Parameter," Phys. Rev. E **49**, 1767-1770 (1994).
11. R. Barer, "Refractometry and Interferometry of Living Cells," J. Opt. Soc. Am. **47**, 545-56 (1957).
12. C. Smithpeter, A. Dunn, R. Drezek, T. Collier, and R. Richards-Kortum, "Near Real Time Confocal Microscopy of Cultured Amelanotic Cells: Sources of Signal, Contrast Agents and Limits of Contrast," J. Biomed. Opt. **3**, 429-36 (1998).
13. H.D. Young. *Statistical Treatment of Experimental Data*. (McGraw-Hill, New York, NY, 1962).
14. H. van de Hulst. *Light Scattering by Small Particles*. (Dover, New York, NY, 1957).

#14701 - $15.00 US Received November 09, 1999; Revised December 14, 1999

15. R. Kudo, S. Sagae, O. Hayakawa, E. Ito, E. Horimoto, and M. Hashimoto, "Morphology of Adenocarcinoma *in Situ* and Microinvasive Adenocarcinoma of the Uterine Cervix. A Cytologic and Ultrastructural Study," Acta Cytol. **35**, 109-16 (1991).
16. N. Wheeler, S. C. Suffin, T. L. Hall, and D. L. Rosenthal "Predictions of Cervical Neoplasia Diagnosis Groups. Discriminant Analysis on Digitized Cell Images," Analyt. Quant. Cytol. Histol. **9**, 169-81 (1987).
17. E. Artacho-Perula, R. Roldan-Villalobos, J. Salas-Molina, and R. Vaamonde-Lemos, "Histomorphometry of Normal and Abnormal Cervical Samples," Analyt. Quant. Cytol. Histol. **15**, 290-97 (1993).
18. L. Burke, D. A. Antonioli, B. S. Ducatman, *Colposcopy. Text and Atlas*, (Appleton & Lance, CA 1991).
19. A. Dunn, C. Smithpeter, A.J. Welch, R. Richards-Kortum, "FDTD Simulation of Light Scattering from Single Cells," J. Biomed. Optic. 2, 262-66 (1997).
20. R. Drezek, A. Dunn, and R. Richards-Kortum, "Light Scattering from Cells: Finite-Difference Time-Domain Simulations and Goniometric Measurements," Appl. Opt. **38**, 3651-3661 (1999).
21. J.R. Mourant, J.P. freyer, A.H. Hielscher, A.A. Eick, D. Shen, and T.M. Johnson, "Mechanism of Light Scattering from Biological Cells Relevant to Noninvasive Optical-Tissue Diagnostics," Appl. Opt. **37**, 3586-3593 (1998).
22. A. Brunsting and P.F. Mullaney, "Differential Light Scattering from Spherical Mammalian Cells," Biophys. J. **14**, 439-453 (1974).
23. J.M. Schmitt and G. Kumar, "Optical Scattering Properties of Soft Tissue: a Discrete Particle Model," Appl. Opt. **37**, 2788-2797 (1998).
24. S. Asano and M. Sato, "Light Scattering by Randomly Oriented Spheroidal Perticles," Appl. Opt. **19**, 962-974 (1980).

1. Introduction

Approximately 1,200,000 people will be diagnosed with cancer in 1999 resulting in 563,000 deaths. The majority of these cancers will be of epithelial origin [1]. Early detection of pre-invasive epithelial neoplasia has the potential to increase patient survival and improve quality of life. However, many of the currently available screening and detection techniques for epithelial pre-cancers do not provide adequate sensitivity and specificity; furthermore, many screening and detection methods require extensive training to yield adequate clinical results. Thus, more sensitive and cost-effective screening and diagnostic techniques are needed to identify curable pre-cancerous lesions.

Pre-cancers are characterized by increased nuclear size, increased nuclear/cytoplasmic ratio, hyperchromasia and pleomorphism, which currently can only be assessed through invasive, painful biopsy. Elastic light scattering spectroscopy may provide a non-invasive tool to assess nuclear morphometry. The wavelength dependence of elastic light scattering is determined by scatterer sizes and refractive indices. Previous work using suspensions of polystyrene spheres and Intralipid with optical properties similar to tissue has shown that the sizes of scattering particles can be estimated from elastic scattering spectra using Mie theory [2]. Recently this principle was applied to estimate distribution of nuclear size in the epithelium of the esophagus [3]. In these experiments, tissue was illuminated with unpolarized light, and the spectrum of reflected light was measured. The reflected light consisted of both singly scattered light originating from the epithelial cells as well as a much stronger multiply scattered component produced in the stroma, which was modulated by hemoglobin absorption. The contributions of the background were modeled and subtracted from the experimental reflectance spectra in order to extract the relatively weak single scattering produced by epithelial cells. The accuracy of this approach depends strongly on the ability of the model to describe the scattering and absorption properties of the stromal layer. Thus, it is highly desirable to develop experimental techniques that would allow the elastic light scattering of epithelial cells to be measured directly.

Previous attempts to optically image skin using polarized illumination and detection suggest that this approach may provide a tool to selectively measure the singly scattered light associated with the epithelium. Reflectance from the skin surface and the light diffusely scattered by the underlying dermis can be separated when polarized illumination and detection are used [4, 5]. When skin is illuminated with linearly polarized light and viewed through a linear polarizer aligned parallel to the polarization of the incident light, surface texture and details are enhanced. When viewed through a linear polarizer aligned perpendicular to the polarization of the incident light, blood vessels and pigmented lesions beneath the skin surface can be seen. In this paper, we explore the use of polarization sensitive light scattering

#14701 - $15.00 US Received November 09, 1999; Revised December 14, 1999

spectroscopy to directly measure the size-dependent elastic light scattering from the upper epithelial layer. We show that this approach can reduce the contributions of multiple scattering and hemoglobin absorption produced by the stroma. A similar approach was recently tested on tissue phantoms consisting of suspensions of polystyrene spheres and cell monolayers placed atop a gel containing mixtures of $BaSO_4$ and human blood [6].

The propagation of polarized light through tissue and turbid media has been addressed in a number of recently published works [7-10]. When polarized light penetrates deep into a tissue it is multiply scattered and, thus, loses its original polarization. A part of this light returns to the surface producing depolarized multiple scattering and another part is absorbed by hemoglobin giving rise to characteristic valleys at 420, 540 and 580 nm. In contrast, light which undergoes a few scattering events in the upper epithelial layer preserves its polarization. Here, we measure the wavelength dependence of scattering with polarization parallel and perpendicular to the polarization of the illumination light. To extract the size-dependent characteristics of scatterers, the perpendicular component of scattered light is subtracted from the parallel one. Mie theory calculations are used to describe the observed scattering spectra and to estimate the sizes of the scatterers. We examine samples of progressively increasing complexity beginning with suspensions of polystyrene beads, progressing to cells, cervical biopsies and finally to *in vivo* oral cavity mucosa. We show that polarization sensitive light scattering spectroscopy has potential to provide direct information about the size distribution of nuclei *in vivo*.

2. Methods

2.1 Instrumentation

A block diagram of the reflectance spectrometer with polarized illumination/detection is shown in Figure 1.

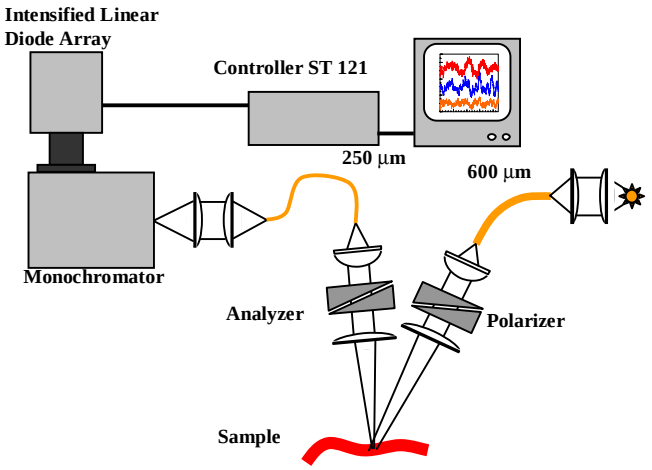

Fig. 1. A diagram of spectrometer used for reflectance measurements with polarized illumination/detection.

Excitation light from a halogen lamp source (Dolan-Jenner Industries) is coupled into a 600 μm core diameter fused silica optical fiber (NA 0.22, Fiberguide Industries). The light delivered by the fiber is collimated, passes through a linear polarizer, and is focused on a sample by a lens with focal distance f = 60 mm. The scattered light is collected and coupled into a 250 μm core diameter fused silica optical fiber (NA 0.22, Fiberguide Industries) using

#14701 - $15.00 US Received November 09, 1999; Revised December 14, 1999

two lenses with f = 40 mm and f = 16 mm, respectively. A linear polarizer-analyzer is placed between the two lenses to measure the scattered light with polarization perpendicular or parallel to the polarization of the illumination light. The collected signal is focused on the 250 μm entrance slit of a single grating spectrograph (f/3.8, 300 lines/mm grating, Monospec 18, Jarrel Ash) coupled to an intensified phodiode array detector (IRY-700, Princeton Instruments). A PC computer controls data acquisition. All lenses used in the set-up are plano-convex fused silica lenses. A mercury lamp (ORIEL) was used to provide a wavelength calibration for the spectrometer. The system's spectral resolution was measured from the width of He-Ne 543.5 nm and 632.8 nm lasers and was found to be *ca.* 5 nm. A constant angle of 36° was maintained between the excitation and collection arms. The light was collected from the middle of the illuminated spot on the sample. The polarization of the excitation light was perpendicular to the plane formed by the excitation and the collection arms. In other words the illumination light was perpendicular to the scattering plane. Collection times and powers used are summarized in Table 1.

2.2 Samples

We measured light scattering spectra from samples of progressively increasing complexity designed to mimic squamous epithelial tissue, which consists of multiple layers of epithelial cells atop a network of stromal collagen. We began by placing either polystyrene spheres or squamous epithelial cells atop a strongly scattering substrate and progressed to cervical

Table 1. Summary of collection parameters and fitting procedures for samples studied.

Sample	Collection Parameters (time/power)	Mie Theory Calculations	
		Fixed Parameters	Parameters Varied*
Polystyrene Beads (water/glycerol)	40-80 sec/370 μW	Diameters of beads, refractive indices of beads and solutions (water and glycerol)	Only k_1, k_2 and *DC*
Cells in BSA	300 sec/370 μW	Mean diameter and distribution of nuclear sizes	Refractive indices of the nuclei and the surrounding medium (cytoplasm); k_1, k_2 and *DC* for nuclei
Cells in PBS	300 sec/370 μW	Mean diameters and distributions of nuclear and cytoplasm sizes; refractive indices of nuclei, cytoplasm and the medium (water)	k_1, k_2 and *DC* for both the nuclei and the cytoplasm
Cells in AA	300 sec/370 μW	Mean diameter and distribution of nuclear sizes; refractive index of the medium (cytoplasm)	Refractive index of nuclei; k_1, k_2 and *DC* for nuclei.
Cervical Biopsies	200 sec/370 μW	Refractive indices of nuclei and cytoplasm	Mean diameters of nuclei and cytoplasm; k_1, k_2 and *DC* for both the nuclei and the cytoplasm
In vivo oral mucosa	60 sec/370 μW	Refractive indices of nuclei and the medium (cytoplasm)	Mean diameter of nuclei; k_1, k_2 and *DC* for nuclei

***** Coefficients for backward (k_1), forward (k_2) Mie scattering components and *DC* offset were always varied to achieve the best fits.

#14701 - $15.00 US Received November 09, 1999; Revised December 14, 1999

biopsies, and finally to *in vivo* oral mucosa. Polystyrene beads (5 μm and 10 μm diameter) were purchased from Bangs Laboratories. SiHa cells (cervical epithelial cancer cells) were kindly provided by Dr. Reuben Lotan from the University of Texas M.D. Anderson Cancer Center.

Suspensions of 5 μm beads in water or glycerol and 10 μm beads in glycerol (100 – 200 μl) were placed atop a diffusely scattering substrate (SRS-99, Labsphere). The substrate strongly depolarizes polarized excitation light and mimics the multiple scattering produced in the stromal layer of epithelial tissue. Glycerol was used to decrease the relative refractive index of the beads from about 1.2 (water) to 1.08 (glycerol) and to provide a viscous environment which prevented the beads from settling during the course of the experiment. The concentration of 5 μm polystyrene beads was chosen so that the beads would approximately form a monolayer if they all settled down on the surface of the substrate. The same concentration (beads per ml of solution) was used in experiments with 10 μm spheres. To prevent beads from aggregating, 3 mg/ml of bovine serum albumin (BSA) were added to the water solution.

A monolayer of 5 μm beads was also formed atop the same diffusely scattering substrate. To prepare the monolayer, the stock solution of 5 μm beads (10%, w/w) was first diluted in ethanol by a factor of *ca.* 40. Then a 50 μl drop of the suspension was placed directly on the surface of the substrate and was allowed to dry. Capillary forces play the major role in formation of the monolayer. This technique produce large areas of highly packed uniformly distributed polystyrene spheres. The quality of prepared monolayers was monitored using a light microscope (Olympus) in reflectance. To measure reflectance spectra in a liquid environment a drop of water was gently added on the top of the monolayer.

Next, cervical epithelial cells were used in place of polystyrene beads. A cell has two distinct interfaces that scatter light: a cytoplasmic membrane and a nuclear membrane. Two approaches were used to characterize the scattering associated with nuclei. First, a high concentration of bovine serum albumin (BSA) was used to match the refractive index of the cytoplasm with the refractive index of the surrounding medium [11]. This effectively eliminates the cytoplasm as an optical interface and allows the scattering of nuclei to be directly assessed. Next, acetic acid (AA) was added to a cell suspension to selectively enhance scattering of nuclei [12]. SiHa cells (cervical epithelial cancer cells) were received in culture medium and were first washed three times in PBS buffer. Then they were divided into three equal aliquots. Cells in each aliquot were allowed to settle and were resuspended in three different solutions: a pure isotonic PBS buffer, a 20 % (g per 100 ml) BSA in PBS, and a 3 % (v/v) acetic acid in PBS.

Four frozen normal cervical biopsies were obtained from Cooperative Human Tissue Network (CHTN). Biopsies were thawed in PBS buffer for about 5-15 minutes immediately before the reflectance measurements. PBS buffer was periodically added to the samples to keep them from drying during the course of experiments.

A normal volunteer was recruited at the University of Texas at Austin for *in vivo* reflectance measurements of oral cavity mucosa. Informed consent was obtained and the study was reviewed and approved by the Internal Review Board of the University of Texas at Austin.

2.3 Data Analysis

Reflectance measurements were made from samples consisting of suspensions of scatterers atop the multiply scattering substrate. For each sample, scattered light was measured with polarization parallel and perpendicular to the polarization of the illumination light. Dark current was recorded and subtracted from all measured spectra. Then the depolarization ratio (D) was calculated (Equation 1):

#14701 - $15.00 US Received November 09, 1999; Revised December 14, 1999

$$D(\lambda) = \frac{I_{II}(\lambda) - I_{\perp}(\lambda)}{I_{II}(\lambda) + I_{\perp}(\lambda)} \quad (1)$$

where $I_{II}(\lambda)$ is the component of the scattered light with polarization parallel to the incident light and $I_{\perp}(\lambda)$ is the component with polarization perpendicular to the incident light and λ is the wavelength of the incident light.

Reflectance measurements were also made from the biopsy and the *in vivo* oral mucosa. The depolarization ratio can not be directly used to assess the scattering characteristics of the epithelial layer in the cervical biopsies and in the *in vivo* measurements because both the parallel and the perpendicular components of the reflectance spectrum have strong contributions from hemoglobin absorption that dominate the depolarization ratio spectrum. Instead the perpendicular component of light scattered by cervical or oral epithelium was first subtracted from the parallel component and the result was normalized to the total intensity of light (the perpendicular plus the parallel components) collected from a diffuse scattering substrate alone. The normalization accounts for spectral characteristics of the excitation lamp and the spectrometer.

2.4 Theoretical Model

To understand the behavior of scatterers placed atop a diffusely scattering substrate, we first need to describe the scattering properties of the substrate alone. Our data show that for the substrate alone, the intensity of light scattered with polarization parallel to the polarization of the illumination light is about 6% higher than that with polarization in the perpendicular direction. Thus, although most of the light is depolarized after scattering from the substrate surface, a small portion of light undergoes single scattering events and preserves the original polarization (Figure 2, left). Thus, the scattering from the substrate alone can be described by equations (2 and 3):

$$I_{II\,S}(\lambda) = I_0(\lambda)S(\lambda)\frac{\Delta\theta}{2\pi} + \frac{1}{2}I_0(\lambda)M(\lambda)\frac{\Delta\theta}{2\pi} \quad (2)$$

$$I_{\perp S}(\lambda) = \frac{1}{2}I_0(\lambda)M(\lambda)\frac{\Delta\theta}{2\pi} \quad (3)$$

Here $I_0(\lambda)$ is the intensity of the illumination light, $I_{IIS}(\lambda)$ and $I_{\perp S}(\lambda)$ are the light scattered by the substrate with polarization parallel and perpendicular to the polarization of the illumination light, $S(\lambda)$ and $M(\lambda)$ are the probabilities of light undergoing single and multiple scattering, respectively, and $\Delta\theta$ is the collection solid angle of our experimental setup. We assume that light is scattered isotropically in the substrate. Since all light undergoes scattering, the sum of $S(\lambda) + M(\lambda)$ must be one:

$$S(\lambda) + M(\lambda) = 1 \quad (4)$$

When a suspension of scatterers of thickness l is introduced atop the diffusely scattering substrate a number of scattering processes can occur (Figure 2, bottom). The illumination beam is backscattered and forward scattered as it travels through the suspension of scatterers, preserving its polarization (Figure 2, I and II). The forward scattered light and the portion of the illumination light that does not undergo any scattering events reach the substrate where they undergo single and multiple scattering. The singly scattered light can undergo single forward scattering events as it travels back through the suspension of scatterers (Figure 2, III)

#14701 - $15.00 US Received November 09, 1999; Revised December 14, 1999

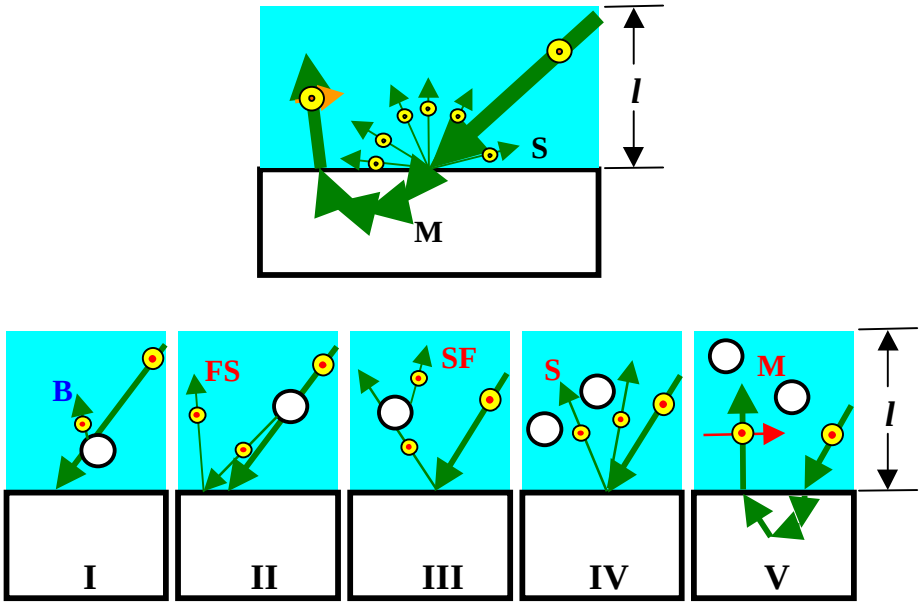

Fig. 2. Schematic presentation of polarized light scattering from diffusely scattering substrate alone (top) and from spherical scatterers placed atop the substrate (bottom). Five different types of scattering events (I-V) can take place and are described in the text.

or reach a detector without undergoing additional scattering events (Figure 2, IV). This portion of the light is still polarized in the same direction as the polarization of the illumination light. We assume that only single scattering events are likely in a suspension of scattering particles. This is a reasonable assumption, considering that in our experiments the total amount of scatterers in a suspension corresponds to one monolayer coverage in the case of polystyrene beads and a few monolayers in the case of cervical cells. Subsequent scattering events of the multiply scattered light do not change its randomized polarization (Figure 2, V). Taking into account the above assumptions, the scattered light which preserves the original polarization, I_{IIB}, can be written as equation (5) where each of the five terms represents the type of scattering depicted in the same order as in Figure 2:

$$I_{IIB}(\lambda) = I_0(\lambda)B(\lambda)Cl + \frac{\Delta\theta}{2\pi} I_0(\lambda)F(\lambda)S(\lambda)Cl(1-Cl\sigma(\lambda)) + \frac{\Delta\theta}{2\pi} I_0(\lambda)S(\lambda)F(\lambda)Cl(1-Cl\sigma(\lambda)) + \frac{\Delta\theta}{2\pi} I_0(\lambda)S(\lambda)\left(1-Cl\sigma(\lambda)\right) + \frac{1}{2} I_0(\lambda)M(\lambda)\frac{\Delta\theta}{2\pi}(1-Cl\sigma(\lambda)) \quad (5)$$

$$F(\lambda) = \int_{\Delta\theta f} P(\lambda,\theta)\sin\theta d\theta \quad (6)$$

$$B(\lambda) = \int_{\Delta\theta b} P(\lambda,\theta)\sin\theta d\theta \quad (7)$$

#14701 - $15.00 US
Received November 09, 1999; Revised December 14, 1999

where $B(\lambda)$ and $F(\lambda)$ are the wavelength dependent cross-sections for backward and forward scattering of light by a single scattering particle, respectively obtained by intergrating the angular dependent scattering cross-section $P(\lambda,\theta)$ (equations 6 and 7). The backscattering cross-section $B(\lambda)$ is calculated for the range of collection angles $\Delta\theta b$ = 139°-149° degree and the forward scattering cross-section $F(\lambda)$ is calculated over $\Delta\theta f$ = (-5°)-(5°). The term $\sigma(\lambda)$ is the total scattering cross-section for a single scattering particle, and C is the number of scatterers per unit volume. Similarly, the scattered light polarized orthogonal to the illumination polarization, $I_{\perp B}(\lambda)$, can be described as equation (8):

$$I_{\perp B}(\lambda) = \frac{1}{2} I_0(\lambda) M(\lambda) \frac{\Delta\theta}{2\pi} (1 - Cl\sigma(\lambda)) \tag{8}$$

Thus, the depolarization ratio is given by equation (9). We take into account only terms linear in $F(\lambda)$, $B(\lambda)$ and $\sigma(\lambda)$ because we assume that only single scattering events occur in the top layer:

$$\frac{I_{IIB}(\lambda) - I_{\perp B}(\lambda)}{I_{IIB}(\lambda) + I_{\perp B}(\lambda)} = \frac{\frac{2\pi Cl}{\Delta\theta} B(\lambda) + ClS(\lambda)F(\lambda) + ClS(\lambda)[F(\lambda) - \sigma(\lambda)] + S(\lambda)}{1 + \frac{2\pi Cl}{\Delta\theta} B(\lambda) + Cl[2S(\lambda)F(\lambda) - \sigma(\lambda)]} \tag{9}$$

The scattering cross-sections of individual particles are much smaller than 1 and in these experiments the concentrations and pathlengths were small. Even for polystyrene beads in water, with the largest relative index (n_{rel}= 1.2) of all samples studied, we can approximate:

$$1 + \frac{2\pi Cl}{\Delta\theta} B(\lambda) + Cl[2S(\lambda)F(\lambda) - \sigma(\lambda)] \approx 1 \tag{10}$$

Thus, we can rewrite the depolarization ratio as:

$$\frac{I_{IIB}(\lambda) - I_{\perp B}(\lambda)}{I_{IIB}(\lambda) + I_{\perp B}(\lambda)} \approx \frac{2\pi Cl}{\Delta\theta} B(\lambda) + ClS(\lambda)F(\lambda) + ClS(\lambda)[F(\lambda) - \sigma(\lambda)] + S(\lambda) \tag{11}$$

All the scatterers studied here were highly forward scattering, where $F \cong \sigma$, so $F\text{-}\sigma \approx 0$. Our data also show that the term $SS(\lambda)$ does not strongly depend on wavelength and can be approximated by a constant. Taking this into account, we obtain equation (12) for the depolarization ratio of scatterers on atop a diffusely scattering substrate:

$$\begin{aligned} \frac{I_{IIB}(\lambda) - I_{\perp B}(\lambda)}{I_{IIB}(\lambda) + I_{\perp B}(\lambda)} &\approx \frac{2\pi Cl}{\Delta\theta} B(\lambda) + ClS(\lambda)F(\lambda) + S(\lambda) = \\ &= k_1 B(\lambda) + k_2 F(\lambda) + DC \end{aligned} \tag{12}$$

which is a linear combination of a forward scattering term, a backward scattering term and a DC offset where $F(\lambda)$ and $B(\lambda)$ are defined in equations (6) and (7).

#14701 - $15.00 US Received November 09, 1999; Revised December 14, 1999

2.5 Mie Theory Calculations

Experimental depolarization ratio spectra were fit to a linear combination of forward and backward scattering terms and a DC offset. Mie theory calculations were used to compute the forward and backward theoretical scattering spectra in the spectral range exploited in these studies. To account for the optical system's finite spectral resolution, computed curves (scattered intensity vs. wavelength) were convolved with a Gaussian of width equivalent to the system's resolution (FWHM=5 nm). Experimental data were then fit to equation (12) using a standard non-negative least squares algorithm to calculate coefficients for forward scattering and backscattering, in addition to a DC offset. The best fits were selected as those with the smallest value of the standard sum of the squared error (SSE). For all fits the χ^2 factors (the goodness of the fits) were calculated. The χ^2 factors indicated that there was at least a 99% chance that the errors were due to random fluctuations [13].

Mie theory calculations were implemented using MATLAB to provide additional flexibility over commercially available Mie software. MATLAB code was verified by comparing results to tabulated curves presented by van de Hulst [14]. For each wavelength, calculations were performed either for a single-sized particle or a Gaussian distribution of particle sizes as noted. Cellular constituents were assumed to be non-dispersive.

2.6 Fitting Procedures for Cells, Biopsies and In Vivo Measurements

Table 1 summarizes the fitting procedures used for different samples.

Cells. In the case of cells in BSA and AA it was assumed that nuclei are the main scatterers and are suspended in a medium with refractive index of cytoplasm. In pure PBS buffer, a cell was treated as consisting of two independent scatterers: a nucleus in an environment with refractive index of cytoplasm and a cytoplasm in an environment with refractive index of water. Thus, depolarization ratio spectra of cells in BSA and AA solutions were fit to a linear combination of three components: forward and backward Mie scattering curves of a nucleus and a DC offset. For cells in PBS solution five components were used: forward and backward Mie scattering terms for both the nucleus and the cytoplasm plus a DC offset.

Mean diameters of cells and nuclei were estimated using phase-contrast microscopy. A Gaussian distribution of diameters was used in the fitting process, Mie theory was used to calculate $B(\lambda)$ and $F(\lambda)$ for the measured size distributions at varying refractive indices. For each combination of Mie theory parameters, a separate least squares fit yielded the coefficients k_1, k_2, DC and the standard sum of the squared error (SSE). The best fit was selected as that with the smallest SSE. First, the best fit was obtained for the depolarization ratio spectrum of cells in BSA. To achieve the best fit, the refractive indices were varied in the range from 1.36 to 1.38 for the surrounding medium and from 1.39 to 1.43 for the nucleus. In this case the refractive index of the surrounding medium corresponds to the refractive index of the cytoplasm. Then, the refractive indices which resulted in the best fit were directly applied to fit the depolarization ratio spectrum of cells in PBS changing only the DC offset and coefficients for forward and backscattering components of both the nucleus and the cytoplasm. The best fit for cells in AA solution was obtained independently varying refractive index of the nucleus from 1.43 to 1.45.

Biopsies and In Vivo Measurements. Refractive indices for the cytoplasm and nucleus derived from the experiments with cells in BSA and PBS solutions were used to fit the depolarization ratio spectra of cervical biopsies and *in vivo* measurements. Here, the mean diameters of the scatterers were varied to achieve the best fits. A Gaussian distribution of sizes was used in Mie theory calculations. A standard deviation (Δ) of nucleus size distribution $\Delta \cong 1$ μm was previously reported in morphometric studies which included two normal sites from cervical epithelium [15]. In a study of cervical epithelial sites with moderate dysplasia (10 cases studied) it was demonstrated that the standard deviation could vary from about 1 μm up to *ca* 4 μm [16]. However, it is known that the deviation of nuclear sizes increases in dysplasia [15-17]. Thus, in the present studies of normal cervical biopsies

#14701 - $15.00 US Received November 09, 1999; Revised December 14, 1999

and normal oral cavity *in vivo* we limited our analysis to distributions with only two standard deviation values Δ = 1 μm and 2 μm to simplify Mie theory calculations.

3. Results

Figure 3 shows the experimental elastic scattering spectra and forward and backward scattering spectra calculated from Mie theory for 5 μm polystyrene beads in water and glycerol and 10 μm beads in glycerol.

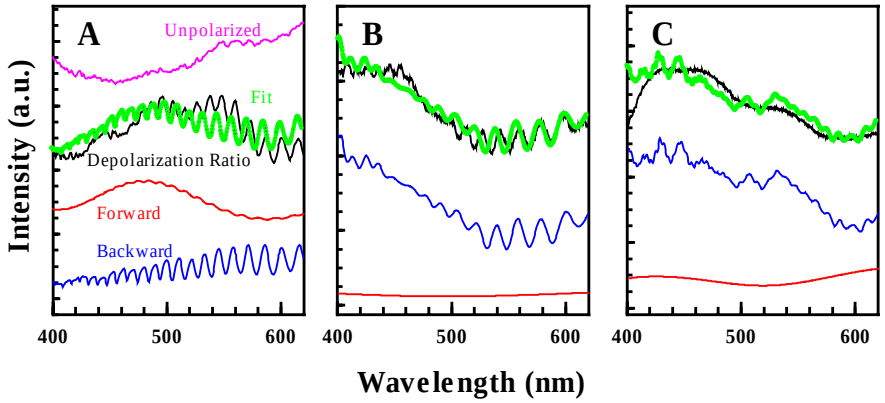

Fig. 3. Reflectance spectra and forward and backward scattering spectra calculated from Mie theory for: 5 μm polystyrene beads in water (A); 5 μm polystyrene beads in glycerol (B); and 10 μm polystyrene beads in glycerol (C). Reflectance spectrum obtained using unpolarized detection is shown in purple; depolarization ratio spectra in black; fits to equation (12) in green; forward components of Mie scattering in red; backscattering Mie components in blue. The theoretical curves are multiplied by coefficients extracted from the least-square algorithm used to achieve the best fits for the experimental data. Arbitrary DC offsets are added to theoretical curves in order to facilitate comparison of all curves on one graph.

First, we compared the spectrum obtained using unpolarized illumination/detection with the depolarization ratio spectrum for 5 μm beads in water (Figure 3 A, purple and black curves, respectively). The spectrum obtained with unpolarized light is dominated by a diffuse background due to multiply scattered light. The depolarization ratios however do show features predicted by Mie theory for 5 μm beads in water as well as for 5 μm and 10 μm beads in glycerol (Figure 3, black curves). The depolarization ratio spectra can be adequately described using a linear combination (Figure 3, green curves) of forward (Figure 3, red curves) and backward scattering (Figure 3, blue curves) components calculated based on Mie theory.

When 5 μm polystyrene beads were self-assembled in a semi-regular monolayer on the surface of the substrate a new periodic component was observed (Figure 4). This periodicity is not described by Mie theory for isolated 5 μm beads in water. The observed periodicity most likely originates from the light scattered in the gaps between the closely spaced polystyrene beads and thus could be related to arrangement of the scatterers in the monolayer.

Figure 5A shows phase-contrast microscopic photographs of cells in different solvents. In PBS, both the cytoplasmic membrane and the nucleus can be clearly seen. In BSA, the cytoplasmic membrane is practically invisible and the contrast of the nuclear membrane is enhanced. After addition of AA, the nucleus decreases in size, probably due to partial dehydration [18] and appears to be much brighter than the surrounding medium, indicating an increase in relative refractive index. Depolarization ratio spectra for cells in the three solutions are shown in Figure 5B with relative intensities preserved. In the presence of BSA (Figure 5B, blue line), scattering from cells is significantly reduced in the red region of the spectrum. Addition of AA results in an overall increase in scattering (Figure 5B, red line).

The depolarization ratio spectrum of cells in BSA was fit to a linear combination of

#14701 - $15.00 US Received November 09, 1999; Revised December 14, 1999

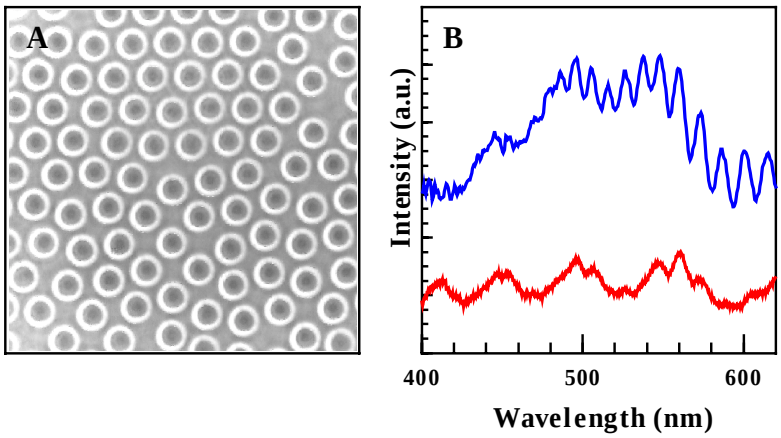

Fig. 4. Density dependence of scattering of 5 μm polystyrene beads in water: (A) a semi-regular monolayer of 5 μm polystyrene beads; (B) depolarization ratio spectra of a water suspension (blue) and of a monolayer of the beads (red).

forward and backward Mie scattering components of nuclei plus a DC offset. The mean diameter of nuclei was determined by light microscopy (d = 12.8 ± 2 μm) and the refractive indices of the nuclei and the surrounding medium were varied to achieve the best fit. The best fit was obtained for relative refractive index of nucleus n_{rel} = 1.036, and medium refractive index, which corresponds to the refractive index of the cytoplasm, n_m = 1.374 (Figure 5C, green curve). The refractive index obtained from the fitting procedure (n_m = 1.374) agrees well with the refractive index of BSA solution used in the experiment (n_m= 1.37).

The refractive indices for nuclei and cytoplasm obtained in the experiments with cells in BSA were directly applied to fit the depolarization ratio spectrum of cells in PBS. The mean diameters of cells (d = 19.0 ± 2 μm) and of nuclei (d = 12.8 ± 2 μm) were determined using phase-contrast microscopy. The best fit was obtained varying only the coefficients for forward and backscattering components of both the nucleus and the cytoplasm and a DC offset value (Figure 5D).

The depolarization ratio spectrum of cells in AA was fit to a linear combination of forward and backward Mie scattering components of nuclei and a DC offset using the mean diameter of nuclei d = 11.0 ± 2 μm. Note that the mean nuclear diameter is smaller than the nuclear diameter in PBS. The refractive index of the surrounding medium n_m = 1.374 was used and the relative refractive index of nuclei was varied. The best fit was obtained for relative refractive index of nuclei n_{rel} = 1.05 (Figure 5E).

Figure 6 illustrates the results obtained for a normal cervical biopsy. Strong hemoglobin absorption is evident in the reflectance spectrum obtained without the polarizer-analyzer in the collection channel (Figure 6A, top curve). The spectrum is normalized to the reflectance from a diffuse scattering substrate to account for spectral characteristics of the excitation lamp and the spectrometer. Both the hemoglobin absorption and the diffuse background were significantly reduced after the parallel and the perpendicular components of the biopsy scattering were collected and the depolarization ratio was calculated (Figure 6A, bottom curve). The resulting scattering profile could be described using Mie theory with the refractive indices derived from the experiments with cells (refractive index of the surrounding media n_m = 1.33, refractive index of cytoplasm n_{cyt} = 1.374, a nucleus-to-cytoplasm relative refractive index n_{rel} = 1.036). It was assumed that both the nucleus and the cytoplasm independently contributed to the scattering of the epithelium. A Gaussian distribution of sizes with standard deviation of 2 μm was used and the mean diameters of cytoplasm and nuclei were varied in Mie theory calculations. The best fit was obtained for the diameter of nucleus d_{nuc} = 8.0 μm and the diameter of cytoplasm d_{cyt} = 19.0 μm (Figure 6B). Note that arbitrary

#14701 - $15.00 US Received November 09, 1999; Revised December 14, 1999

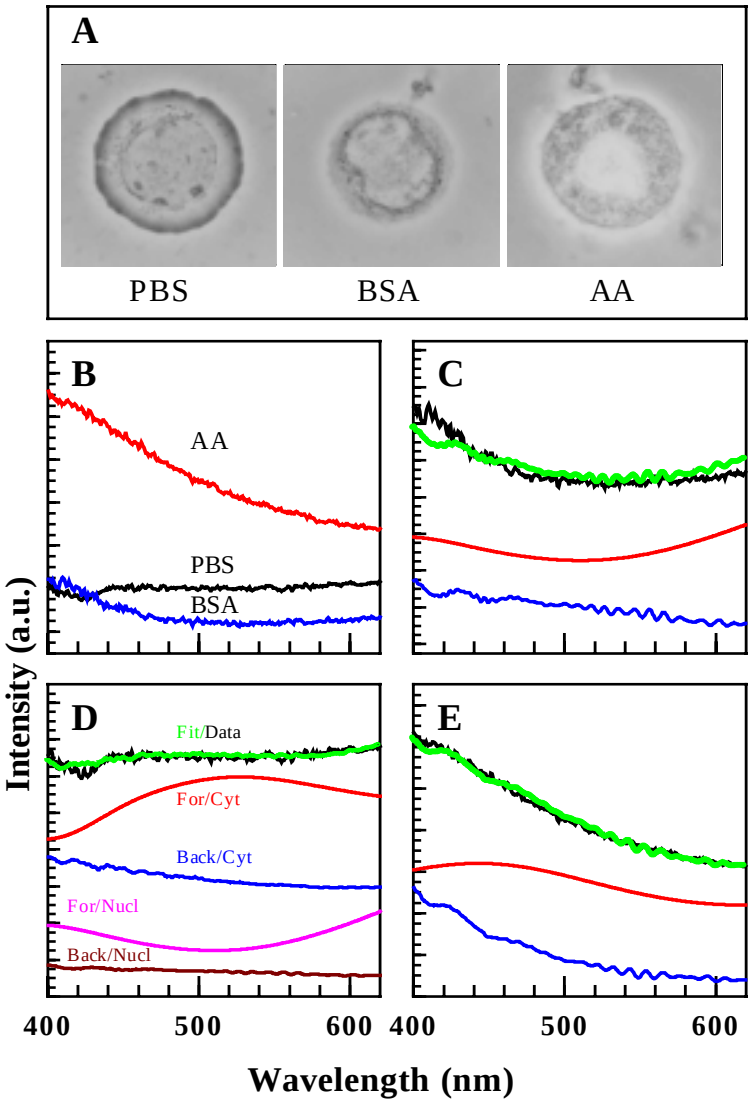

Figure 5. Scattering spectra of SiHa cells: (A) phase-contrast photographs of cells in: a pure PBS buffer (left), BSA/PBS solution that matches the refractive index of the cytoplasm (middle), and acetic acid/PBS solution (right); (B) reflectance spectra of SiHa cells in the presence of acetic acid (red), in the PBS buffer (black), and in the presence of high concentration of BSA (blue). Experimentally measured depolarization ratio spectra and Mie theory calculations for scattering of: (C) cells in BSA/PBS (measured depolarization ratio spectrum – black, the best fit to equation (12) – green, forward Mie scattering component of the nucleus – red, backscattering of the nucleus – blue); (D) cells in PBS (measured depolarization ratio spectrum – black, the best fit to equation (12) – green, forward Mie scattering component of the cytoplasm – red, backscattering of the cytoplasm – blue, forward Mie scattering component of the nucleus – purple, backscattering of the nucleus – brown); (E) cells in acetic acid/PBS (measured depolarization ratio spectrum – black, the best fit to equation (12) – green, forward Mie scattering component of the nucleus – red, backscattering of the nucleus – blue). The theoretical curves are multiplied by coefficients extracted from the least-square algorithm used to achieve the best fits for the experimental data. Arbitrary DC offsets are added to theoretical curves in order to facilitate comparison within one plot.

#14701 - $15.00 US
Received November 09, 1999; Revised December 14, 1999

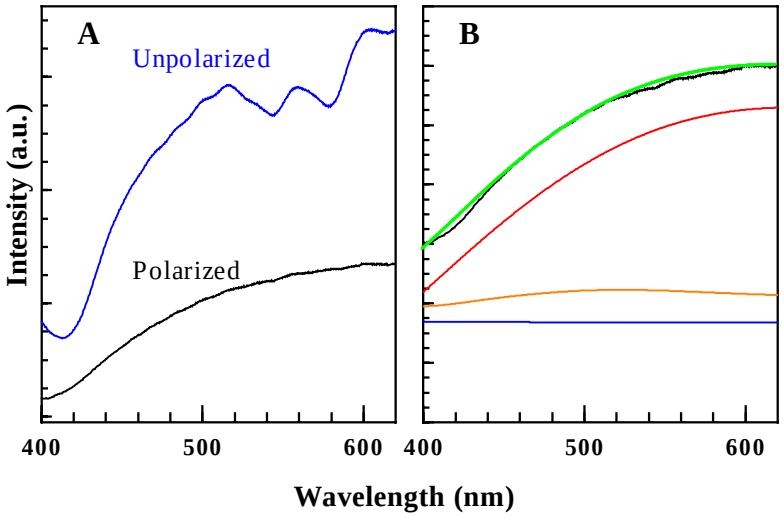

Fig. 6. Measured reflectance spectra and Mie calculations for normal cervical biopsy: (A) reflectance spectra obtained using unpolarized (blue) and polarized (black) illumination/detection; (B) depolarization ratio spectrum (black), calculated fit to equation (12) (green), forward Mie component of nucleus (red), forward Mie component of cytoplasm (orange), and backward Mie component of cytoplasm (blue). The theoretical curves are multiplied by coefficients extracted from the least-square algorithm used to achieve the best fits for the experimental data. Arbitrary DC offsets are added to theoretical curves in order to facilitate comparison within one plot.

DC offsets are added to the theoretical curves presented in Fig. 6 B in order to facilitate their comparison within one plot. It can be seen that the forward Mie component of nucleus closely resembles the experimental depolarization ratio spectrum. Mie theory calculations showed that the contribution of the forward Mie scattering from the nucleus is about 8 times higher relative to the forward component of the cytoplasm. Thus, it can be concluded that the scattering from the epithelium is mainly determined by the scattering from nuclei. The backscattering components of both the nucleus and the cytoplasm were found to be flat and featureless as compare to the forward components. It is important to note that in our model (see Methods) we assumed that the depolarization ratio of the diffusely scattering background from stromal layer is wavelength independent. To confirm this assumption we measured the depolarization ratio of stroma for a normal cervical biopsy and found that it was spectrally flat relative to the depolarization ratio of the epithelial layer.

In vivo measurements of oral cavity mucosa are summarized in Figure 7. As in the case of *in vitro* tissue measurements, the use of polarized illumination/detection significantly reduces the contribution of hemoglobin absorption to the reflectance spectra (Figure 7A, compare blue and black curves). Since our biopsy data suggest that nuclei determine epithelial tissue scattering, only the nucleus was used to fit the scattering profiles obtained *in vivo*. The mean diameter of nuclei was an unknown parameter in Mie theory calculations and was found to be 5 μm. A Gaussian distribution of sizes with 1 μm standard deviation was used.

The nuclear diameters of 8 μm and 5 μm obtained from Mie theory calculations for the cervical biopsy and *in vivo* measurements, respectively, agree reasonably well with previously reported value of 6.1 ± 0.7 μm [17] obtained from morphometric measurements of normal squamous cervical epithelium.

#14701 - $15.00 US
Received November 09, 1999; Revised December 14, 1999

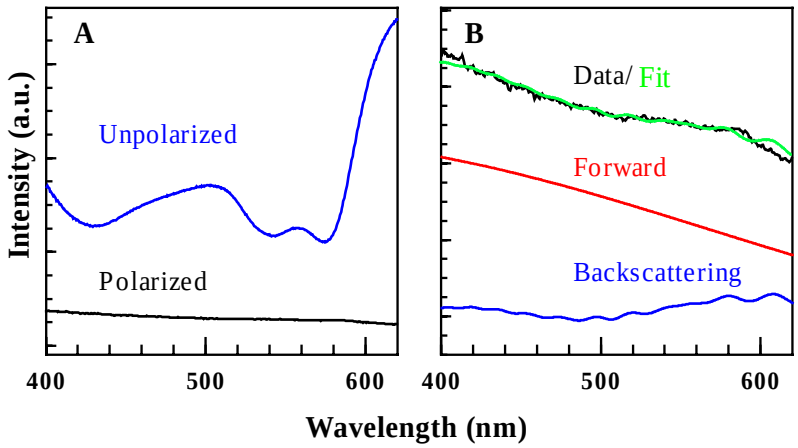

Fig. 7. Oral cavity reflectance spectra obtained *in vivo* and corresponding Mie theory calculations: (A) reflectance spectra obtained using unpolarized (blue) and polarized (black) illumination/detection. (B) Polarized reflectance spectrum (black), calculated fit to equation (12) (green), forward Mie component of scattering of nucleus (red), and backscattering Mie component of nucleus (blue). Arbitrary DC offsets are added to the theoretical curves in order to facilitate comparison within one plot.

4. Discussion and conclusions

Results presented in Figures 6 and 7 demonstrate that polarized reflectance spectroscopy can be used to detect the scattering properties of the epithelial layer in the presence of both a strong diffusely scattering background and hemoglobin absorption. The resulting scattering spectra can be described by Mie theory using nuclear sizes of epithelial cells as unknown parameters. The best fits to experimental data provide information about the nuclear size distribution which is a key quantitative morphologic characteristic used by pathologists in detection of pre-cancerous lesions. The approach proposed here is based on the fact that few scattering events do not significantly alter the polarization of incident light while multiple scattering leads to depolarization. Only few scattering events can occur in the epithelial layer, whereas light that penetrates deeper in the tissue undergoes multiple scattering by stroma as well as absorption by hemoglobin. When polarized excitation is used, the portion of the reflectance spectrum with polarization parallel to the polarization of the illumination light consists of light scattered by epithelial cells and a diffuse background signal from stroma which is modulated by hemoglobin absorption. At the same time the component of the reflectance spectrum with polarization perpendicular to that of the incident light polarization contains only the diffuse background scattering. Thus, the scattering size-dependent characteristics of the epithelial layer can be obtained from the depolarization ratio.

Here, we demonstrate that depolarization ratio spectra can be used to extract size-dependant periodic Mie scattering of polystyrene beads in the presence of much stronger diffuse scattering from the substrate. Polystyrene spheres provide a good first model to study because their sizes and refractive indices are well known and their scattering spectra are well described by Mie theory. Comparison of scattering spectra of diluted suspensions of polystyrene beads with their highly packed semi-regular monolayers revealed a new periodic component which is not described by Mie theory for individual beads. We believe that this periodicity is related to the spacing between beads in the monolayer and, thus, similar behavior could also be observed in other systems consisting of regular spaced scatterers.

Next, we analyzed scattering of cell suspensions whose refractive indices are much smaller than polystyrene beads and whose internal structure is more complex. In general, the exact solution for elastic scattering of light by a cell is determined by the cell size and the three-dimensional distribution of refractive indices inside the cell [19]. However, our results show that scattering from cells can be described using a simplified model where a cell is treated as two independent, spherical scatterers: a nucleus and a cytoplasm which are

#14701 - $15.00 US Received November 09, 1999; Revised December 14, 1999

described using average refractive indices**.** It was shown that the forward scattering of cells can be adequately described using Mie theory calculations with average refractive indices of nucleus and cytoplasm [20-22]. However, the situation is more complicated for backward scattering where the fluctuations of the refractive index inside cell and scattering from organells smaller than nucleus become increasingly important [20, 21, 23]. Unfortunately, very little information is available on these index variations and more work needs to be done before these variations can be adequately taken into account to describe the backscattering of cells. In our model we also assumed that cells and nuclei are spherical objects and, thus, do not depolarize light after a single scattering event. In fact cells are not strictly spherical. For example, it was reported that normal squamous epithelial cervical cells have ellipsoidal shape with major to minor axis ratio of about 1.3 [17]. In general, polarization of light can be altered as a result of backscattering at large angles from ellipsoidal particles with the maximum depolarization effect for ellipsoids with major to minor axis ratio of about 2 [24]. The depolarization decreases as the shape parameter approaches the value of 1 or infinity. However, it was noted that the depolarization is very small for nonspherical particles with a refractive index close to 1 [24]. Recent polarization measurements of tissue phantoms and *in vitro* tissue also indicated that the nonspherical nature of the scatters in biological tissue does not cause major pertubation of polarization in scattering of light [7].

The scattering of cell nuclei can be directly characterized when the optical interface between the cytoplasm and solvent is eliminated using BSA. The best fit provides refractive indices for both the nucleus and the cytoplasm which is the surrounding medium of nuclei. We used the refractive indices obtained from the experiment with cells in BSA solution to describe the scattering of cells in a pure PBS buffer where both the cytoplasm and the nucleus contribute to the reflectance spectrum. Mie theory calculations were in good agreement with the experimental data. This result suggests that cell suspensions in BSA solution could be effectively used to determine refractive indices of different types of cells including cells at different stages of cancer development.

Our interest in scattering properties of cells in the presence of AA is driven by the fact that AA is a commonly used contrast agent in detection of epithelial pre-cancers [18]. Our previous results showed that addition of AA results in an overall increase of nuclear scattering relative to scattering from the cytoplasm [12]. Based on this observation we assumed that nuclei are the main scatterers in cell suspensions in AA solution. Phase-contrast microscopic photographs of cells in AA suggest that the refractive index of nuclei in AA is higher than the refractive index of nuclei in PBS (Figure 5A). Our Mie theory calculations showed that scattering of cells in AA solution can be described if the relative refractive index of nuclei is increased from 1.036 (PBS) to 1.05 (AA).

Dramatic decreases in both the hemoglobin absorption and the diffuse scattering were observed when polarized illumination/detection was used to analyze reflectance spectra of epithelial tissue *in vitro* and *in vivo*. We demonstrate that the resulting scattering spectra can be described using Mie theory calculations with the refractive indices derived from the experiments with cell suspensions in BSA and PBS solutions. Initially, we assumed that both the nucleus and the cytoplasm contribute to the scattering of the epithelium. However, Mie theory calculations for a cervical biopsy showed that nuclei determine the scattering properties of the epithelial layer (Figure 6B, compare black, green and red curves). This result is not unexpected because it is more adequate to treat an epithelial layer which consists of densely packed cells as a continuous medium with refractive index of the cytoplasm and embedded nuclei rather than a suspension of isolated cells. Thus, only nuclei were used to fit polarized reflectance spectra obtained *in vivo* (Figure 7B). The best fits resulted in mean diameters of nuclei which are in good agreement with previously reported morphometric analysis of normal epithelial cells where the mean diameter of about 6.1 ± 0.7 μm [17] were reported. Differences in mean diameters obtained from different sets of measurements could be attributed to individual variations from person to person.

In summary, our results suggest that the use of polarized illumination and detection allows selective detection of the size-dependent Mie scattering of epithelial nuclei *in vivo*.

#14701 - $15.00 US Received November 09, 1999; Revised December 14, 1999

Subsequent analysis of the Mie scattering component can provide information about the nuclear size distribution and nuclear morphometry - key parameters in histopathologic analysis of epithelium which currently can only be assessed through invasive, painful biopsy. Further development of the proposed approach could extend the potential of optical spectroscopic techniques for non-invasive real-time detection of epithelial neoplasia *in vivo*.

Acknowledgements

We acknowledge the Southern Division of Cooperative Human Tissue Network at the University of Alabama at Birmingham for providing human cervical biopsies for these studies. This work was supported by a grant from the National Institute of Health (CA72650).

#14701 - $15.00 US Received November 09, 1999; Revised December 14, 1999